

Nanotechnology E-Newsletter

November 2005

Supercritical fluid deposition of nanowire building blocks

The importance of the information and communication technology (ICT) sector to both the economy and society at large cannot be overstated, and few technologies have as far-reaching societal and economical impacts. The semiconductor industry plays a pivotal role in ICT. In their 2005 Annual Report, the SIA (Semiconductor Industry Association) comments, "The semiconductor industry sets the pace of global economic growth. Just as the industry's strength provides a leading indicator of the world's economic health, advanced semiconductor products and systems are bringing new opportunities, growth, and development to countries around the globe."

Moore's Law is the beating heart at the centre of this industry, driving business growth through the technological realization of new process technologies that double the number of transistors on a chip about every two years. However, as the semiconductor industry continues to miniaturize in following Moore's Law, there are some real challenges ahead, particularly in moving deeper and deeper into the nano length scale.¹ Sustaining the traditional logic MOSFET (metal-oxide-semiconductor field-effect transistor) structure, design, and material composition will be especially difficult beyond 22nm. The next technology standard is a 9nm physical gate length, predicted to be reached in 2016 according to the International Technology Roadmap for Semiconductors, and as early as 2011 according to some company roadmaps.² There is even the question of how far silicon charge-based logic MOSFET transistor devices can be scaled. The semiconductor sector of the ICT industry is therefore actively chasing solutions that can fulfill the Moore criteria.

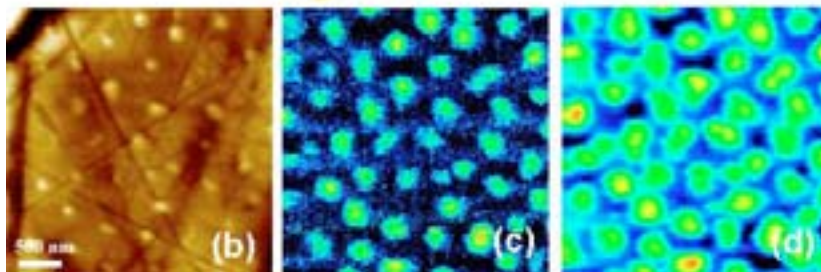
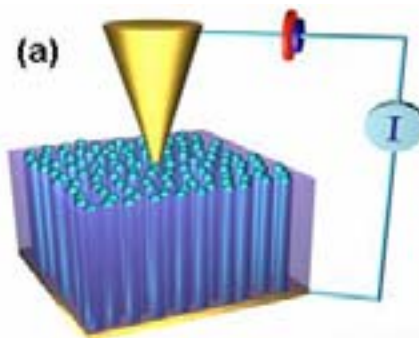


Figure 1. Conductive atomic force microscopy (C-AFM) of Ge nanowires embedded within anodized aluminum oxide (AAO). (a) Representation of the C-AFM, (b) AFM topography of Ge-nanowires-AAO surface, (c) C-AFM current map at 20V and (d) current map at 40V.⁵

In particular, the industry is looking at new materials. Nanowires offer two possible solutions for the given challenge. The first lies in their unique properties, the other in realizing revolutionary, hierarchical, three-dimensional nanoscale architectures and designs not achievable with conventional materials and techniques. At University College Cork, in collaboration with CRANN at Trinity College Dublin, supercritical fluid (SCF) solution phase methods³ have been exploited for forming arrays of semiconductor, metal, and metal oxide nanowires within the channels of porous templates for potential nanoscale device applications.⁴ In this article we report on recent work in our laboratories that demonstrate the flex-

ibility of SCF methods for producing a range of useful, templated, nanowire structures.

Recently we reported the use of SCF techniques to consistently produce high-density, ordered arrays of crystalline germanium nanowires within anodized aluminum oxide (AAO) templates.^{4,5} Conductive atomic force microscopy (C-AFM) and macro-contacting strategies were used to study the electrical properties of the germanium nanowires within these arrays (see Figure 1). Each nanowire was found

to possess similar electrical properties, demonstrating the continuous and reproducible nature of SCF methods.

We also investigated the optical properties of SCF-grown silicon and germanium nanowires within the pores of hexagonal mesoporous silica matrices.⁶ A clear blue-shift in the photoluminescence (PL) of the semiconductor composite material was observed as the diameter of the nanowires decreased from 85Å to 22Å (see Figure 2). Powder X-ray diffraction revealed that, due to escalating lattice expansion, the strain on the crystallographic structure increased as the diameter of the confined nanowires decreased. This resulted in a shift of the PL maximum to higher energies. The ability to manipulate the optical properties of templated semiconductor nanowires through strain engineering has important implications for the design of future optical devices.

Dilute magnetic semiconductor (DMS) materials exhibit semi-conducting properties and long-range ferromagnetic ordering, and is anticipated that these materials will play a vital

Continues on page 2.

Supercritical fluid deposition of nanowire building blocks

Continued from cover

role in the integration of spintronic devices with traditional semi-conducting technologies.⁷ We have reported the synthesis of $\text{Ge}_{1-x}\text{Mn}_x$ ($0 \leq x \leq 0.05$) DMS nanowire arrays with diameters between 35-60nm in AAO templates. These nanowires exhibited room temperature ferromagnetism that is surprisingly high for this class of material.^{7,8} Structural investigations showed that these wires are comprised of a highly crystalline germanium host lattice containing discrete and spatially separated manganese ions.

Additionally, we have realized the integration of magnetic and semi-conducting materials through the synthesis of a range of high-density arrays of coaxial nanocables: such as germanium nanowires surrounded by a cobalt nanotube sheath within AAO (Figure 3).⁹ Structural studies on these heterostructured nanowires have clearly demonstrated the presence of discrete core-shell phases with no evidence of alloy formation. These materials form well-defined building blocks that may lead to new spin-based multifunctional devices.

In conclusion, the adaptability of SCF deposition techniques combined with versatile

templating materials offers the opportunity to synthesize and assemble ordered arrays of orientated nanowire structures that have specific dimensions and controllable electronic, optical, and magnetic properties. Identifying the synthetic parameters to 'dial-up' nanowires with specific properties, in robust and hierarchical templates, could lead to many new and exciting applications of these materials in future devices.

We acknowledge financial support from the Higher Education Authority (HEA) in Ireland, the Irish Research Council for Science Engineering and Technology (IRCSET) and Science Foundation Ireland (SFI). We would also like to acknowledge all collaborators involved with the work, particularly Michael Morris, Donats Erts and Olga Kazakova.

Donna C. Arnold and Justin D. Holmes*
Centre for Research on Adaptive Nanostructures Nanodevices (CRANN)
Trinity College Dublin, Ireland.
*Department of Chemistry
University College Cork, Ireland
E-mail: j.holmes@ucc.ie

References

1. G. E. Moore, *Cramming more components onto integrated circuits*, **Electronics** **38** (8), p. 114, April 1965.
2. **Int'l Technology Roadmap for Semiconductors (ITRS)**, 2003.
3. J. D. Holmes et al., *Control of thickness and orientation of solution-grown silicon nanowires*, **Science** **287**, p. 1471, February 2000.
4. K. J. Ziegler et al., *Conductive films of ordered nanowire arrays*, **J. Mater. Chem.** **14** (4), p. 585, 2004.
5. D. Erts et al., *High density germanium nanowire assemblies: Contact challenges and electrical characterisation*, **J. Mater. Chem.**, submitted.
6. G. Audoit et al., *Strain-induced photoluminescence from silicon and germanium nanowire arrays*, **J. Mater. Chem.**, 2005 (advanced article).
7. J. S. Kulkarni et al., *Structural and magnetic characterisation of $\text{Ge}_{0.99}\text{Mn}_{0.01}$ nanowire arrays*, **Chem. Mater.** **17** (14), p. 3615, July 2005.
8. O. Kazakova et al., *Room-temperature ferromagnetism in $\text{Ge}_{1-x}\text{Mnx}$ nanowires*, **Phys. Rev. B** **72** (9), p. 094415, September 2005.
9. T. A. Crowley et al., *Probing the magnetic properties of cobalt-germanium nanocable arrays*, **J. Mater. Chem.** **15** (24), p. 2408, 2005.

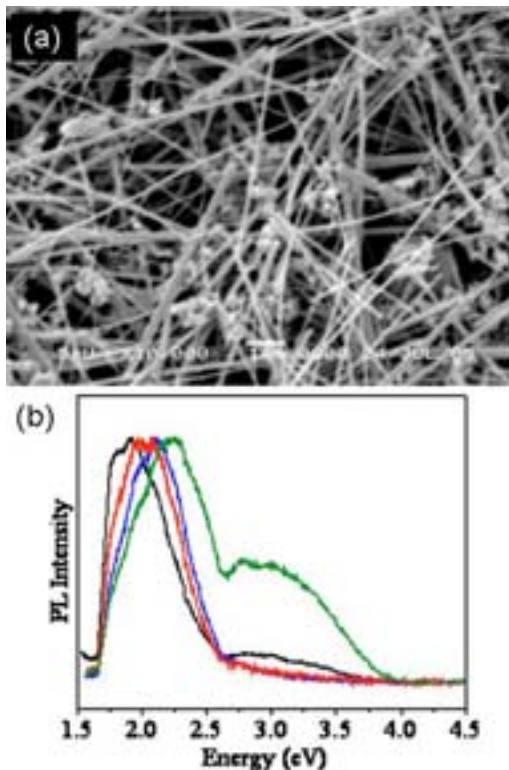


Figure 2. (a) Electron Microscopy image of free-standing Ge nanowires. (b) Solid state PL spectra at room temperature for silicon nanowires with diameters (from left to right) 73Å, 50Å, 45Å and 30Å respectively.⁶

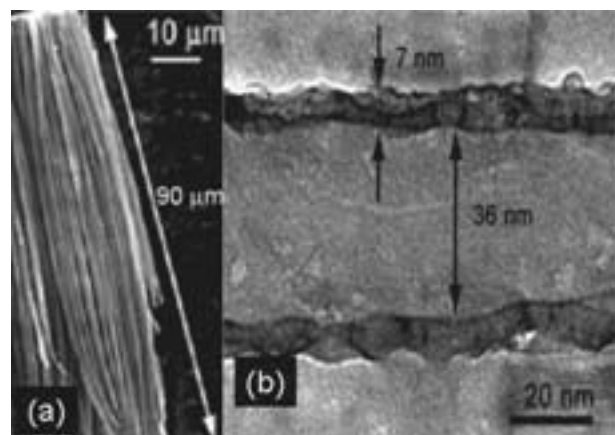


Figure 3. Electron Microscopy images of Co-Ge coaxial nanocables. (a) Scanning electron microscope image of nanocables partially liberated from AAO matrix and (b) Tunneling electron microscope image of a Co nanotube formed within AAO, showing nanotube wall thickness of 7nm.⁹

Femtosecond imaging of surface plasmon dynamics

Light interacting with nanostructured metals excites collective charge density fluctuations known as surface plasmons (SP). Through excitation of SP eigenmodes, incident light is trapped on nanometer spatial and femtosecond temporal scales and its field is enhanced. Excitation of SP resonances leads to extraordinary physical phenomena including the anomalous transmission of light through sub-wavelength aperture arrays¹ and enhancement of nonlinear optical processes. Recently, the prospect of plasmonic devices^{2,3} has stimulated considerable effort to understand the fundamental dynamics of SPs and to develop practical applications such as ultra-sensitive chemical sensors and sub-wavelength optics. The physics of surface plasmons concerns the properties of electromagnetic fields on nanometer spatial and femtosecond temporal scales. The special scale of SPs excited in metal nanoparticles distributes for the order of 10 - 100nm, and the coherent lifetime ranges from a few to tens of femtoseconds.

A new technique demonstrated here enables us to investigate surface plasmon dynamics with sub-femtosecond temporal precision and sub-wavelength spatial resolution.⁴ We combine techniques of interferometric time-resolved two-photon photoemission (ITR-2PP)⁵ with photoelectron emission microscopy (PEEM). Phase-correlated pump and probe optical pulses with 10fs duration excite SP modes in a nano-structured silver film.⁶ Imaging of photoelectrons with electron optics creates a map of SP fields that mediate two-photon photoemission. We present a movie of SP fields at 330as per frame and 50nm spatial resolution—a trillion times faster than conventional techniques.

Figure 1 shows one- and two-photon photoemission (1 and 2PP-PEEM) images of the same part of the silver grating excited with a Hg lamp ($\lambda=254\text{nm}$) and a p-polarized femtosecond laser ($\lambda=400\text{nm}$). The 1PP-PEEM image simply shows a topography of the sample because the 254-nm (4.89eV) light is above the plasmon resonances of silver (bulk plasmon = 3.8eV). By contrast, the 2PP-PEEM image in Figure 1b is dominated by many spikes. Each 'spike' represents a localized surface plasmon that is trapped at a nano-scale defect and oscillating at 750THz (400nm light frequency).

A movie of surface plasmons is recorded by advancing the delay time (τ_d) between pump and probe pulses in $1/4$ optical cycle, or 330as (one optical cycle = $1/(750\text{THz}) = 1.33\text{fs}$). Figure 2 presents selected frames where we extract a portion of each image (highlighted in Figure 1b).⁷ Four dots start to oscillate completely in-phase at the beginning of the movie,

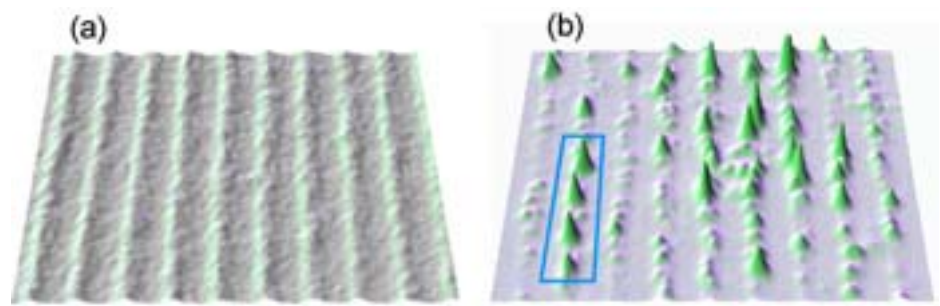


Figure 1. PEEM micrographs of the identical region on a silver grating obtained with (a) the 254nm line of a Hg lamp (1PP-PEEM), and (b) a p-polarized 400nm femtosecond laser excitation (2PP-PEEM). The length of a scale bar is $2\mu\text{m}$.

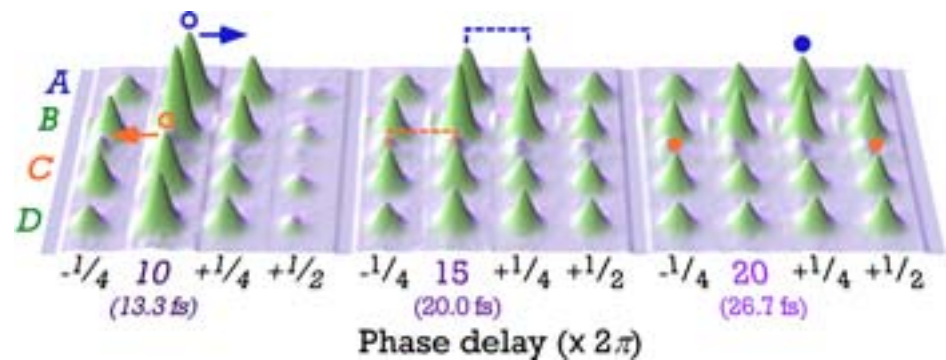


Figure 2. Frames of a movie of the localized surface plasmons highlighted in Figure 1b. The interval of the frame is 0.33fs or $1/4 \times 2\pi$ in terms of the optical phase of the carrier light ($\lambda=400\text{nm}$). As the delay time evolves from $10 \times 2\pi$ to $20 \times 2\pi$, the phase of dot A (C) is retarded (advanced). Markers (blue and orange) indicate the change in the intensity maxima in five cycle intervals.

because the pump pulse introduces coherent oscillations by driving polarizations at the light carrier frequency. After the pump pulse over, each dot starts to oscillate at its characteristic plasmon frequency. The discrepancy in these frequencies causes variations in oscillation phases of dots. As τ_d proceeds from $10 \times 2\pi$ to $20 \times 2\pi$, the phase of the amplitude maximum of dot A is retarded by $1/4 \times 2\pi$, while that of dot C is forwarded by $\sim 1/2 \times 2\pi$, as indicated by blue and orange markers, respectively. This result indicates that the plasmon frequency of dot A is slightly lower than the 400nm light frequency, while that of dot C is slightly higher.

Figure 2 also constitutes a realization of quantum control: we specify excitation and de-excitation of individual dots with sub-femtosecond accuracy by tuning excitation fields through a choice of τ_d . With more complex methods, it is now possible to engineer control fields with arbitrary spatial and tempo-

ral phase.⁸ By using such engineered optical fields, we can control the spatio-temporal evolution of plasmon fields within systems of metallic and semiconductor nanostructures. The quantum control of coherent excitations in such photonic devices with complex ultrafast $<10\text{-fs}$ optical pulses could be the basis for optical information processes with 100-THz bandwidth. The ability to image the time-evolution of SP fields by the interferometric time-resolved PEEM technique opens the way for us to study the dynamical properties of nanophotonic devices.

This research has been supported by NSF DMR-0116034 and NSF ECS-0403865 grants. A. K. acknowledges fellowship support from the Yamada Science Foundation of Japan.

Continues on page 4.

Femtosecond imaging of surface plasmon dynamics

Continued from page 3.

Atsushi Kubo, Ken Onda, Hrvoje Petek†, Zhijun Sun*, Yun S. Jung* and Hong Koo Kim*

*Department of Electrical Engineering and Institute of NanoScience and Engineering
Department of Physics and Astronomy and Institute of NanoScience and Engineering
University of Pittsburgh, Pittsburgh PA

†Corresponding author.

E-mail: petek@pitt.edu

References

1. T. W. Ebbesen, H. J. Lezec, H. F. Ghaemi, T. F. Ghaemi, T. Thio, and P. A. Wolff, *Extraordinary optical transmission through sub-wavelength hole arrays*, **Nature** **391**, p. 667, 12 February 1998.
2. W. L. Barnes, A. Dereux, and T. W. Ebbesen, *Surface plasmon subwavelength optics*, **Nature** **424**, p. 824, 14 August 2003.
3. R. P. Van Duyne, *Molecular Plasmonics*, **Science** **306**, p. 985, 5 November 2004.
4. A. Kubo, K. Onda, H. Petek, Z. Sun, Y. S. Jung, and H. K. Kim, *Femtosecond Imaging of Surface Plasmon Dynamics in a Nanostructured Silver Film*, **Nano Lett.** **5** (6), p. 1123, 17 May 2005.
5. H. Petek and S. Ogawa, *Femtosecond time-resolved two-photon photoemission studies of electron dynamics in metals*, **Prog. Surf. Sci.** **56** (4), p. 239, December 1997.
6. Z. Sun, Y. S. Jung, and H. K. Kim, *Role of surface plasmons in the optical interaction in metallic gratings with narrow slits*, **Appl. Phys. Lett.** **83** (15), p. 3021, 13 October 2003.
7. Movies of surface plasmons are available at <http://pubs.acs.org/journals/nalefd/> as supporting information.
8. T. Feurer, J. C. Vaughan, and K. A. Nelson, *Spatiotemporal coherent control of lattice vibrational waves*, **Science** **299**, p. 374, 17 January 2003.

Gold nanoparticles for cancer cell imaging and photothermal therapy

The development of nanoparticles with different structures and shapes has created widespread interest in their potential use in diagnostic imaging and therapy applications. Gold nanoparticles have potential for biological applications due to their easy preparation, size and shape, controlled optical properties, and great biocompatibility. They strongly absorb and scatter visible and near-infrared light and provide a novel contrast agent for simultaneous molecular imaging and photothermal cancer therapy. Recently, gold nano-shells have been reported for this application that have a silica core covered with a thin shell of gold: they operated in the near-infrared region because of their strong near-infrared absorption.¹ However, the silica core in the nanoshell could be toxic. Gold nanoparticles, on the other hand, are well known to be safe in vivo application: when they are conjugated with anti-EGFR antibodies they can be used for cancer cell diagnostics under illumination of a beam of white light² and can also be used for selective photothermal therapy of cancer cells using visible lasers.³

Gold nanoparticles of 35nm in diameter are conjugated with anti-EGFR monoclonal antibodies. One benign epithelial cell line, HaCaT (human keratinocytes), and two malignant epithelial cell lines (human oral squamous cell carcinoma, HOC 313 clone 8 and HSC 3) were cultured on 18mm diameter glass cover in DMEM plus 5% FBS at 37°C under 5% CO₂. The cell monolayer was incubated with the anti-EGFR/Au conjugates in buffer for 40 minutes at room temperature and then fixed with paraformaldehyde and sealed with another cover slip with a small amount of glycerol. The cells were imaged in dark field using an inverted Olympus IX70 microscope. The high numerical dark field condenser (U-DCW) delivers a very narrow beam of white light from a tungsten lamp and the

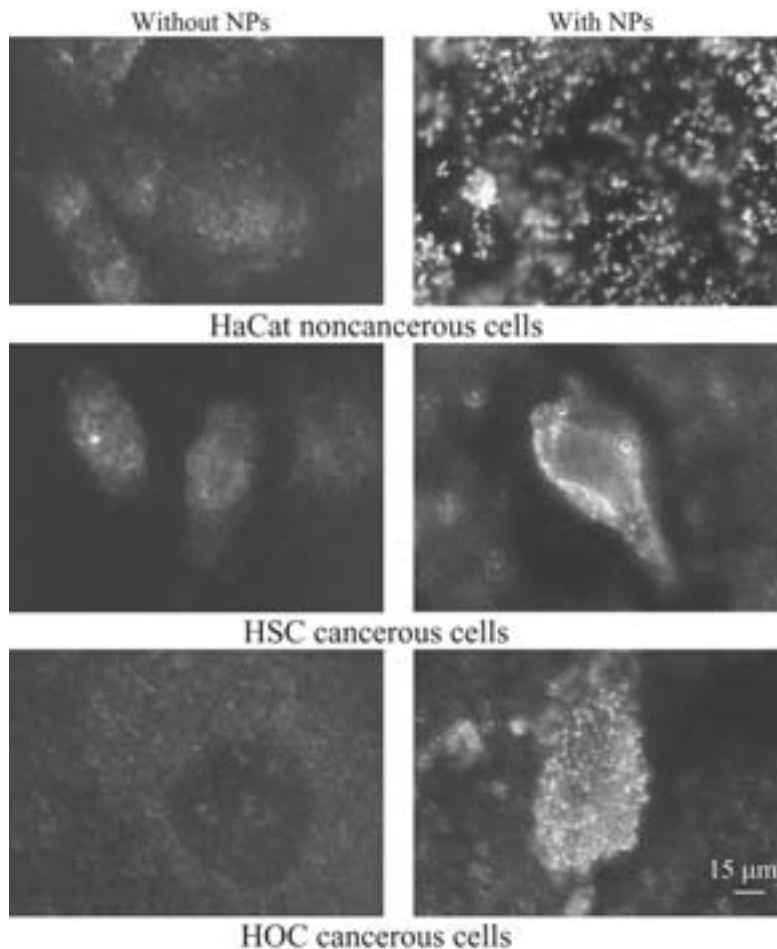


Figure 1. Light-scattering images from gold nanoparticles in cancer diagnostics: images of HaCaT noncancerous cells (top row), of HSC cancerous cells (middle row) and of HOC cancerous cells (bottom row) without gold nanoparticles (left column) and with anti-EGFR antibody conjugated gold nanoparticles (right column). The light scattering images of cancerous and noncancerous cells shows obvious difference due to the specific and stronger binding of the antibody conjugated gold nanoparticles to cancerous cells.

100x /1.35 oil Iris Ph3 objective (UPLANAPO) collect only the scattered light from the samples.

Figure 1 shows the light scattering images of the three types of cells with and without incubation with anti-EGFR/Au conjugates. The light scattering pattern of gold nanoparticles in cancerous and noncancerous cells is significantly different when anti-EGFR antibodies are conjugated to gold nanoparticles. The HaCaT noncancerous cells are poorly labeled with the nanoparticles and the cells could not be identified individually. When the conjugates are in-

cubated with HOC and HSC cancerous cells for the same amount of time, the nanoparticles are obviously bound to the surface of the cells in higher amounts. This contrast difference is due to the specific binding of overexpressed EGFR on the surface of the cancer cells with the anti-EGFR antibodies bound to the gold surface. The nanoparticles are also found on the HaCaT noncancerous cells in small amounts due to the nonspecific interactions between the antibodies and the proteins on the cell surface: thus the nanoparticles are randomly distributed on the whole cell monolayer. The nonspecific interaction is also reflected in the broadening and red shift of the absorption band of the gold nanoparticles on the non-cancerous cells.²

Due to the specific binding of anti-EGFR/Au conjugates to the cancer cells, it is possible to selectively kill the cancer cells by conversion of the photo energy absorbed by gold nanoparticles into local heat energy. In our work, a CW argon laser at 514nm with different energies was used to irradiate the cells after incubation with anti-EGFR/Au conjugates. The overlapping of the laser wavelength with the surface plasmon absorption band of gold nanoparticles around 520nm enables efficient absorption of the laser energy. Cell viability was tested by

staining with 0.4% trypan blue, which will accumulate inside dead cells but is pumped out of live ones.

Figure 2 shows the images of all cells with and without nanoparticles after irradiation. Without nanoparticle incubation (left column), neither cancerous nor noncancerous cells were killed at the highest energy we used: 75W/cm². After incubation with the anti-EGFR-antibody-conjugated gold nanoparticles, all three types of cells showed photo-destruction damage, but

Continues on page 6.

Gold nanoparticles for cancer cell imaging and photothermal therapy

Continued from page 5.

at different laser energies (right two columns). After exposure to the argon laser at and above $57\text{W}/\text{cm}^2$, all HaCaT noncancerous cells within the laser spots were photo-damaged and shown in deep black color due to the uptake of trypan blue, while at lower energy values only a few or no cells were damaged. The HSC cancerous cells were photo-destroyed at a much lower power density. Cell death occurred within the laser spots after exposure at and above $25\text{W}/\text{cm}^2$ while no cell deaths were observed at a lower power density than $19\text{W}/\text{cm}^2$. The HOC malignant cells also underwent photothermal destruction at a much lower power density than required for HaCaT benign cells. Cell death within the laser spots was observed at and above $19\text{W}/\text{cm}^2$. These results show that gold nanoparticles can be used for selective cancer-cell therapy with a simple, visible, continuous-wave laser.

For the clinical application of treating can-

cer in vivo under the skin, near-infrared laser light is necessary because it has larger penetration depth.⁴ Using the technique described here we are able to tune the absorption band of the nanoparticles to the near-infrared region by changing the shapes of the nanoparticles. Thus, selective cancer-cell therapy in the near-infrared region is possible.⁵

Xiaohua Huang, Ivan H. El-Sayed* and Mostafa A. El-Sayed

Laser Dynamics Laboratory
School of Chemistry and Biochemistry
Georgia Institute of Technology, Atlanta, GA

*Department of Otolaryngology—Head and Neck Surgery

University of California at San Francisco
Comprehensive Cancer Center
San Francisco, CA

E-mail: mostafa.el-

sayed@chemistry.gatech.edu

References

1. C. Loo, A. Lowery, N. Halas, J. West, and R. Drezek, *Immunotargeted nanoshells for integrated cancer imaging and therapy*, **Nano Lett.** **5** (5), p. 709, 2005.
2. I. H. El-Sayed, X. Huang, and M. A. El-Sayed, *Surface Plasmon Resonance Scattering and Absorption of anti-EGFR Antibody Conjugated Gold Nanoparticles in Cancer Diagnostics: Applications in Oral Cancer*, **Nano Lett.** **5** (5), p. 829, 2005.
3. I. H. El-Sayed, X. Huang, and M. A. El-Sayed, *Selective laser photo-thermal therapy of epithelial carcinoma using anti-EGFR antibody conjugated gold nanoparticles*, **Cancer Lett.**, to appear.
4. R. Weissleder, *A clearer vision for in vivo imaging*, **Nat. Biotechnol.** **19**, p. 316, 2001.
5. X. Huang, I. H. El-Sayed, W. Qian, and M. A. El-Sayed, *Cancer cell imaging and photothermal therapy in NIR region by using gold nanorods*, **JACS**, submitted.

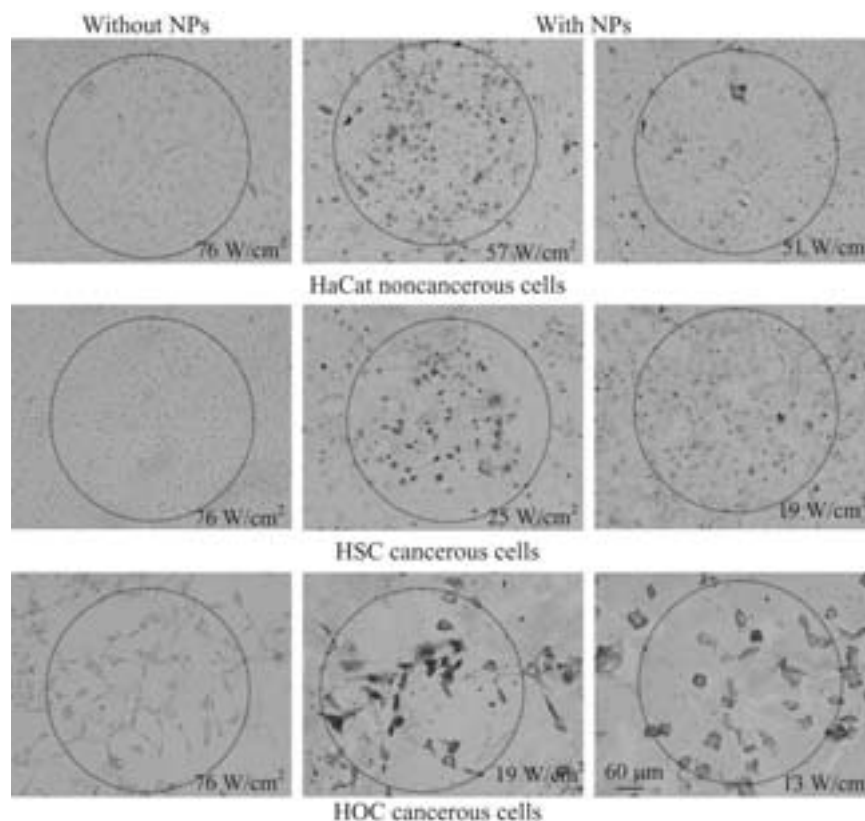


Figure 2. Selective laser photothermal cancer therapy: HaCaT noncancerous (top row), HSC cancerous cells (middle row) and HOC cancerous cells (bottom row) irradiated at different laser powers without (left column) and with (right two columns) nanoparticles. HaCaT noncancerous cells were killed at and above $57\text{W}/\text{cm}^2$ while cancerous cells were killed at much lower laser powers ($19\text{--}25\text{W}/\text{cm}^2$ and above).

Controllable switching of carbon nanotube emission energies

Single walled carbon nanotubes (SWNTs) are remarkable molecules being explored for applications in conductive composites, molecular electronics, biological markers, and chemical sensors. SWNTs can be visualized as single sheets of graphite wrapped into nanometer-diameter tubes, and exhibit a range of electronic behaviors from metallic to semi-conducting. The diverse electronic structure of different species depends on the wrapping vector of the graphite sheet, and optical methods have been particularly helpful in classifying SWNTs.¹

Techniques such as absorption, Raman, and photoluminescence (PL) spectroscopy have attracted considerable interest as tools for studying SWNT electronic properties. In addition to being able to probe large nanotube ensembles optically, we can also look at isolated, individual SWNTs.^{2,3} Recently, we reported abrupt shifts in the photoluminescence energy of individual single-walled carbon nanotubes caused by increased absorption of laser light above a certain threshold.⁴ This effect is likely linked to laser induced absorption/desorption of ambient gas molecules binding to the walls of the nanotube. Other groups have shown gas effects on SWNTs using electrical detection schemes,^{5,6} and an all-optical 'readout' of a chemical sensing nanotube may have significant implications for sensory applications. Moreover, it appears reasonable that charge injection of electron-hole pairs should be able to trigger the shift, which may have certain opto-electronic applications.

Photoluminescence is a process in which a photon is emitted as an electron and hole radiatively recombine from an optically-excited, metastable state. For SWNTs, one finds that PL emission energies can be combined with higher energy absorption resonances to identify different tube species.⁷ Nonetheless, our understanding of optical emission from carbon nanotubes is still in a somewhat nascent

state. For example, a consensus is forming that SWNT PL is dominated by excitonic recombination, although free carrier recombination is still discussed. Additionally, there appears to be some disagreement between the emission energies measured by different methods, an effect which seems to be linked to differences in dielectric environment between nanotubes in solution and those suspended in air. In addition, some sideband transitions have been observed but not yet identified.

To obtain PL from individual tubes, we grow SWNTs by chemically assisted vapor deposition (CVD) over micron-sized holes in a silicon nitride membrane. Transmission electron microscopy of the apertures confirms the presence of individual SWNTs bridging the open areas. PL is collected from the suspended SWNTs using a confocal microscope with a tunable excitation source and a motorized sample stage.

By rastering the stage and collecting PL spectra from each sample position, we obtain diffraction-limited images that probe the spatial dependence of PL emission on excitation position. At low excitation power, the tubes behave as expected and emit PL at a single peak wavelength. At higher laser intensity, however, the spatial image unexpectedly changes and 'holes' appear in the middle of the image. At these sample positions the PL emission peak has suddenly blueshifted about 20meV (Figure 1a). By imaging at the blueshifted peak energy (Figure 1b), the complementary spatial image is produced and corresponds to the 'missing' region in Figure 1a. Example PL spectra from the unshifted and blueshifted regions are given in Figure 1c.

The blueshifted regions grow with increased absorption into the tube as determined by raising the laser power, co-aligning the excitation light with the tube axis, or by bringing the excitation energy into resonance with the tube's absorption peak.

These results establish a link between a photon absorption threshold and the threshold for the blueshifted PL spectra. Our work additionally shows that the shifts can be triggered by optical excitation of certain 'hot spots' along the nanotube, as seen in Figure 1 where two foci are observed in the spatial images.

Our calculations indicate that laser heating of the tube may raise the nanotube temperature sufficiently for gas desorption, causing a blueshift in the PL spectra. Parallel work on large ensembles of nanotubes by Finnie *et al.*, has kept the excitation power constant but varied the sample temperature. These latter studies have conclusively related similar band-gap shifts to desorption of gases.⁸ Together, the results suggest that control of adsorbates is essential for obtaining 'native' optical properties

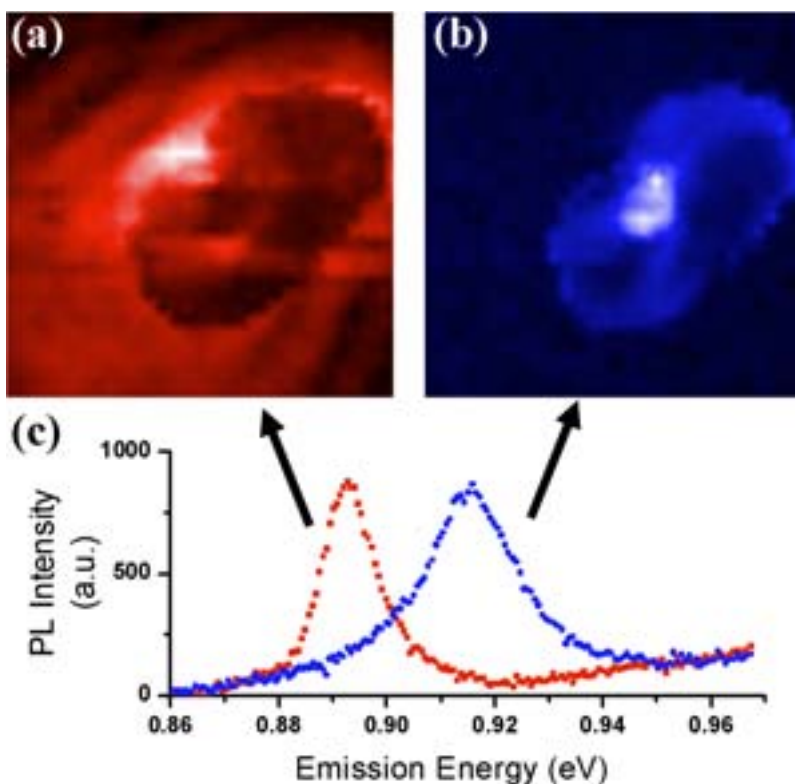


Figure 1. A $3 \times 3 \mu\text{m}$ spatial map of the photoluminescence (PL) intensity at the peak (a) unshifted and (b) blueshifted emission energies. The 'hole' in the middle of part a of the figure corresponds with an increase in the PL intensity at the blueshifted emission energy as seen in part b. (c) Examples of the unshifted (red squares) and blueshifted (blue circles) PL spectra.

Continues on page 8.

Controllable switching of carbon nanotube emission energies

Continued from page 7.

of carbon nanotubes. Our work suggests that one route could be through laser-induced desorption of adsorbates from a nanotube that is initially at low temperature and pressure. A laser pulse could be used to momentarily heat the nanotube by hundreds of degrees, removing adsorbates and permitting studies of 'bare' nanotube properties once cryogenic temperatures are restored.

**D. E. Milkie, C. Staii, S. Paulson,
E. Hindman, A. T. Johnson, and
J. M. Kikkawa**

Department of Physics and Astronomy
University of Pennsylvania, Philadelphia, PA

References

1. R. Saito, G. Dresselhaus, and M. S. Dresselhaus, **Physical Properties of Carbon Nanotubes**, Imperial College Press, London, 1999.
2. A. Hartschuh, H. N. Pedrosa, L. Novotny, and T. D. Krauss, *Simultaneous Fluorescence and Raman Scattering from Single Carbon Nanotubes*, **Science** **301**, p. 1354, 5 September 2003.
3. J. Lefebvre, Y. Homma, and P. Finnie, *Bright Band Gap Photoluminescence from Unprocessed Single-Walled Carbon Nanotubes*, **Phys. Rev. Lett.** **90**, p. 21740, 30 May 2003.
4. D. E. Milkie, C. Staii, S. Paulson, E. Hindman, A. T. Johnson, and J. M. Kikkawa, *Controlled Switching of Emission Energies in Semiconducting Single-Walled Carbon Nanotube*, **Nano. Lett.** **5**, p. 1135, 18 May 2005.
5. J. Kong, N. R. Franklin, C. Zhou, M. G. Chapline, S. Peng, K. Cho, and H. Dai, *Nanotube Molecular Wires as Chemical Sensors*, **Science** **287**, p. 622, 28 January 2000.
6. E. S. Snow, F. K. Perkins, E. J. Houser, S. C. Badescu, and T. L. Reinecke, *Chemical Detection with a Single-Walled Carbon Nanotube Capacitor*, **Science** **307**, p. 1942, 25 March 2005.
7. S. M. Bachilo, M. S. Strano, C. Kittrell, R. H. Hauge, R. E. Smalley, and B. R. Weisman, *Structure-Assigned Optical Spectra of Single-Walled Carbon Nanotubes*, **Science** **298**, p. 2361, 20 December 2002.
8. P. Finnie, Y. Homma and J. Lefebvre, *Band-Gap Shift Transition in the Photoluminescence of Single-Walled Carbon Nanotubes*, **Phys. Rev. Lett.** **94**, 24741, 24 June 2005.

Join the Nanotechnology Technical Group

Please Print Prof. Dr. Mr. Miss Mrs. Ms.

First Name, Middle Initial, Last Name _____

Position _____ SPIE Member Number _____

Business Affiliation _____

Dept./Bldg./Mail Stop/etc. _____

Street Address or P.O. Box _____

City/State _____ Zip/Postal Code _____ Country _____

Telephone _____ Telefax _____

E-mail Address/Network _____

Technical Group Membership fee is \$30/year, or \$15/year for full SPIE members.

- Nanotechnology
Total amount enclosed for Technical Group membership \$ _____
- Check enclosed.** Payment in U.S. dollars (by draft on a U.S. bank, or international money order) is required. Do not send currency. Transfers from banks must include a copy of the transfer order.
- Charge to my:** VISA MasterCard American Express Diners Club Discover
- Account # _____ Expiration date _____
- Signature _____
(required for credit card orders)

Expand the area and scope of your knowledge by connecting directly with others in your field. SPIE Technical Groups bring colleagues together to communicate new ideas, approaches, and challenges, not just in one country or once a year, but all over the world, all the time.

As a technical group member you will:

- Keep pace with rapid change through focused information from SPIE.
- Gain contacts in your industry with an online membership directory.
- Network with colleagues at conferences and special events.
- Influence future technical activities within SPIE.

Prepare for what's next in your field and in your career. Join today!

Send this form (or photocopy) to:
SPIE • P.O. Box 10
Bellingham, WA 98227-0010 USA
Tel: +1 360 676 3290
Fax: +1 360 647 1445
E-mail: spie@spie.org

Please send me

- Information about SPIE Membership
 Information about other SPIE technical groups
 FREE technical publications catalog

Reference Code: 4171

Nanotechnology

This e-newsletter is published quarterly by SPIE—The International Society for Optical Engineering.

<i>Editor</i>	Sunny Bains	<i>Managing Editor</i>	Rich Donnelly
<i>Editorial Assistant</i>	Stuart Barr	<i>Graphic Designer</i>	Linda DeLano

Editorial Board Members:

David Andrews, Univ. of East Anglia; **James Grote**, Air Force Research Lab; **Jonathon Howard**, Max Planck Institute and Univ. of Washington; **Laszlo Kish**, Texas A&M University; **Akhlesh Lakhtakia**, Pennsylvania State Univ.; **Christi Madsen**, Bell Labs, Lucent Technologies; **Nils Peterson**, Nat'l Inst. for Nanotechnology, Univ. of Alberta; **Paras Prasad**, State Univ. of NY at Buffalo; **Mike Sailor**, Univ. of California at San Diego; **Richard Silver**, National Institute of Standards

Articles in this newsletter do not necessarily constitute endorsement or the opinions of the editors or SPIE.

SPIE is an international technical society dedicated to advancing engineering, scientific, and commercial applications of optical, photonic, imaging, electronic, and optoelectronic technologies. Its members are engineers, scientists, and users interested in the development and reduction to practice of these technologies. SPIE provides the means for communicating new developments and applications information to the engineering, scientific, and user communities through its publications, symposia, education programs, and online electronic information services.

Copyright ©2005 Society of Photo-Optical Instrumentation Engineers. All rights reserved.

SPIE—The International Society for Optical Engineering, P.O. Box 10, Bellingham, WA 98227-0010 USA.
 Tel: +1 360 676 3290. Fax: +1 360 647 1445.

European Office: Karin Burger, Manager, karin@spieeurope.org, Tel: +44 7974 214542. Fax: +44 29 2040 4873.

In Russia/FSU: 12, Mokhovaja str., 119019, Moscow, Russia • Tel/Fax: +7 095 202 1079
 E-mail: edmund.spierus@relcom.ru